Research Article Vol. 37, No. 6 / June 2020 / Journal of the Optical Society of America A 995

Journal of the Optical Society of America A

OPTICS, IMAGE SCIENCE, AND VISION

New C_n^2 statistical model based on first radiosonde turbulence observation over Lhasa

Yajuan Han,[1,2] Xiaoqing Wu,[1,*] Tao Luo,[1] Chun Qing,[1] Qike Yang,[1,2] Xiaomei Jin,[1] Nana Liu,[1,3] Su Wu,[1,2] and Changdong Su[1,2]

[1]Key Laboratory of Atmospheric Optics, Anhui Institute of Optics and Fine Mechanics, Chinese Academy of Sciences, Hefei, Anhui 230031, China
[2]Science Island Branch of Graduate School, University of Science and Technology of China, Hefei, Anhui 230031, China
[3]School of Environmental Science & Optoelectronic Technology, University of Science and Technology of China, Hefei, Anhui 230026, China
*Corresponding author: xqwu@aiofm.ac.cn

Received 3 January 2020; revised 7 April 2020; accepted 23 April 2020; posted 27 April 2020 (Doc. ID 387211); published 20 May 2020

It is worth highlighting that, for the first time to the best of our knowledge, vertical profiles of atmospheric parameters and C_n^2 were measured at Lhasa, south of the Tibetan Plateau, using balloon-borne radiosondes. Based on the measurements, two new statistical models (Lhasa HMN and Lhasa Dewan) for estimating turbulence strength are proposed. Attention has been paid to evaluate the reliability of the two models to reconstruct vertical profiles of C_n^2 from a statistical perspective. The statistical analyses presenting the Lhasa HMN model are accompanied with lower bias, root mean square error (RMSE), and bias-corrected RMSE (σ) than those of the Lhasa Dewan model, which implies the Lhasa HMN model can better reveal the nature of turbulence characteristics of Lhasa influenced by unique local weather conditions. In addition, the comparison between the Lhasa HMN model and measurements in calculating integrated astroclimatic parameters is carried out, and the result suggests that the performance of the Lhasa HMN model is reliable and satisfactory. The new reliable C_n^2 model offers new insight into the characteristics of optical turbulence at Lhasa and provides support for pursuing astronomical site selection in the Tibetan Plateau.

https://doi.org/10.1364/JOSAA.387211

1. INTRODUCTION

Optical turbulence generates due to the occurrence of local inhomogeneities in the atmosphere, especially for the spatial inhomogeneities of temperature, which further leads to random fluctuation of the refractive index [1]. Optical turbulence affects observation through an astronomical telescope by limiting image quality, interfering with the propagation of laser beams and so on. The effects can be described by the refractive index structure constant (C_n^2) [2,3]. Therefore, appropriate knowledge of vertical profiles of C_n^2 and further understanding of optical turbulence characteristics are essential for improving the performance of adaptive optics (AO) systems.

To avoid the influence of optical turbulence, global astronomers have been searching for suitable places to conduct astronomical observations. Astronomical site selection is a long-term and grueling process, which requires major human power, material resources, and financial resources. In order to deploy powerful facilities for astronomical observations, it is necessary to carry out a large number of investigations on astronomical locations. In terms of site selection, the Tibetan Plateau (TP) has attracted the interest of astronomers around the world because of its high plateaus with an average altitude of more than 4500 m and its unique nature phenomena and weather conditions. In 2012, Richard Stone indicated that Ali, west of the TP, was likely an international observatory on the "Roof of the World" for Asia [4]. Thus far, some investigations have been carried out in TP, e.g., Ali [5–10], Nagqu [11], Tingri [12], and Qamdo [13]. Lhasa (91.13°E, 29.67°N) is located in the south of the TP, with an altitude of about 3650 m above sea level (a.s.l.). The location and height distribution of Lhasa, as well as the above-mentioned four sites (Ali, Nagqu, Tingri, and Qamdo) are shown in Fig. 1. Previous studies [14–16] showed that Lhasa had satisfactory meteorological qualifications for astronomical applications, such as little cloud cover, low precipitation, and high annual sunshine time over 3000 h. Moreover, Wang *et al.* [17] investigated the integrated astroclimatic parameters in the TP; the results showed that Lhasa had good free atmosphere visibility and large wavefront coherence time, which are favorable for telescope observations. Therefore, Lhasa is a promising site for astronomical observations and should be explored in the future.

In view of the importance of Lhasa in astronomical site selection, only possessing knowledge of simple meteorological conditions would be insufficient. In order to investigate the site performance, it is critical to obtain different turbulence profiles and to analyze the turbulence characteristics. However, up to

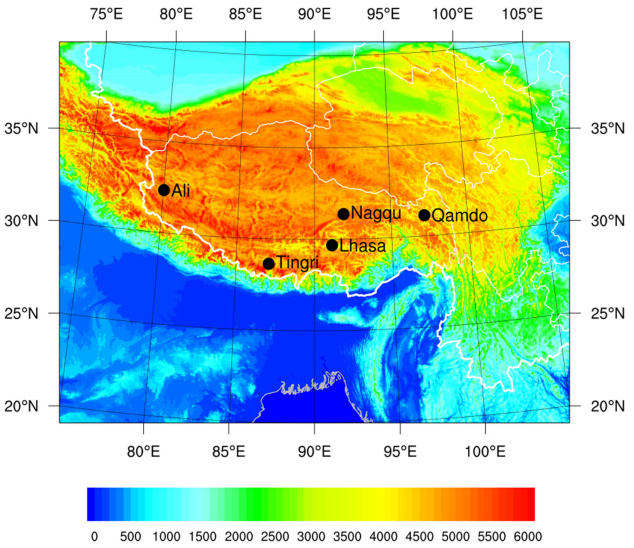

Fig. 1. Topographic map (altitude in meters) of the Tibetan Plateau; black dots denote Lhasa, Ali, Nagqu, Tingri, and Qamdo.

Fig. 2. Balloon-borne radiosonde is launched at Lhasa Meteorological Station.

now, there are no *in situ* measurements of vertical profiles of C_n^2 and classical meteorological parameters at Lhasa.

Therefore, in August 2018, as a preliminary survey, we acquired the vertical distribution of atmospheric temperature (T), atmospheric pressure (P), relative humidity (RH), wind speed, wind direction, and C_n^2 profiles at Lhasa using balloon-borne radiosondes for the first time. The aim of the study is to present a more precise statistical outer scale model to estimate the turbulence strength of Lhasa and deepen our understanding of the characteristics of atmospheric turbulence in the TP. This will lay a foundation for the astronomical site selection in the TP by using classic meteorological parameters to estimate turbulence profiles and combining with a mesoscale atmospheric model.

In this study, the performance of Colman–Vernin (C-V), HMNSP99 (HMN), and Dewan models in estimating optical turbulence strength is evaluated by six balloon samples at Lhasa. Based on the measurements, we present two new statistical outer-scale models, named Lhasa HMN and Lhasa Dewan, which calculate C_n^2 profiles from atmospheric parameters. Utilizing the two new models, comparisons of turbulence intensity at Lhasa between models and measurements have been carried out. Statistical analyses between the measurements and model-based estimations are carried out to evaluate the level of reliability of the Lhasa HMN and Lhasa Dewan models. Moreover, the Lhasa HMN model is used to predict the Fried parameter (r_0), the seeing (ε), the isoplanatic angle (θ_0), and the wavefront coherence time (τ_0) at Lhasa.

2. EXPERIMENTS AND PRINCIPLE OF METEOROLOGICAL BALLOON

A. Experiment Details

From August 3 to 18, 2018, a field campaign of balloon-borne radiosondes equipped with micro-thermometers and GPS was conducted by the Anhui Institute of Optics and Fine Mechanics, Chinese Academy of Sciences at Lhasa Meteorological Station, south of the TP. All of the flights were released during the early morning or late evening in local time, as shown in Fig. 2. Specific flight information is listed in Table 1.

Table 1. Record of Meteorological Balloons at Lhasa Used in the Study[a]

Balloon Number	Launch Date	Launch Time	Termination Time	Termination Altitude/m
1#	2018.08.08	19:16	20:38	26900.7
2#	2018.08.13	19:23	20:29	23221.1
3#	2018.08.14	19:40	21:05	30657.1
4#	2018.08.15	07:24	08:51	30217.7
5#	2018.08.16	19:19	20:43	31206.4
6#	2018.08.17	07:00	08:23	29068.0

[a]Time is local time. Altitude is a.s.l. in m.

The vertical profiles of C_n^2, structure function parameter for temperature (C_T^2), P, T, RH, wind speed, and wind direction were obtained. The ascent rate of the balloon is 6 m/s, and the vertical resolution is about 30 m. A micro-thermometer is crucial equipment for detecting atmospheric parameters, as shown in Fig. 3. Here, the frequency response range of the micro-thermometer is 0.1–30 Hz, the corresponding statistical average time is 5 s, and the equivalent noise of temperature fluctuation is about 0.002°C [18–20].

The average profiles of C_n^2 and corresponding atmospheric parameters measured by meteorological balloons are depicted in Fig. 4. For ease of description, the height above ground level (a.g.l.) is reported in all figures in the paper. According to the temperature profile, the tropopause appears at around 14 km a.g.l. The wind speed increases with height, reaching the maximum around 24 km a.g.l., which is approximate 26 m/s. The wind direction fluctuates greatly from the ground up to 10 km a.g.l. and tends to be stable above 10 km a.g.l. The turbulence strength near the ground is strong. Generally speaking, a strong

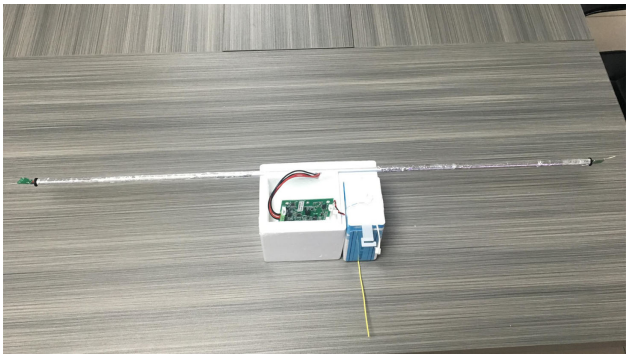

Fig. 3. Equipment of micro-thermometer used in balloon-borne radiosonde.

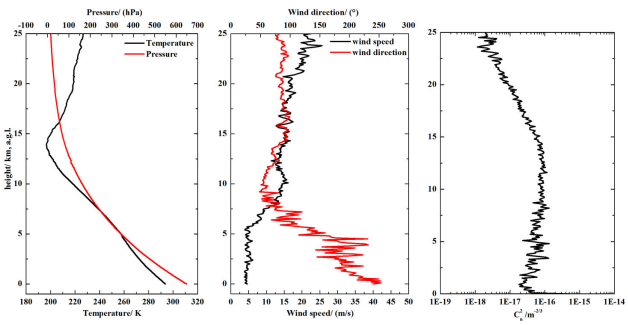

Fig. 4. Average profiles of atmospheric temperature, pressure, wind speed, wind direction, and C_n^2 measured by six samples of meteorological balloons. On the y axis, the height a.g.l. is reported.

turbulence layer appears at around the tropopause. However, it is not obvious at Lhasa.

B. Principle of C_n^2 Measurement

The two thin-wire resistance temperature sensors of the micro-thermometer are made of platinum wire with a diameter of 10 μm and a length of 20 mm. The sensors detect the temperature difference caused by atmospheric temperature and further response to resistance. There is a significant linear correlation between temperature difference and sensor resistance. The distance between the two sensors can be viewed as the arms of the Wheatstone bridge. Later, the Wheatstone bridge converts resistance changes into voltage changes. Therefore, we can obtain the proportionality coefficient between voltage changes and temperature changes according to Eq. (1):

$$\Delta V = A \cdot \Delta T. \tag{1}$$

Temperature structure function $D_T(r)$ is influenced by the temperature difference of two micro-thermometer sensors with a horizontal distance r, as defined by Eq. (2):

$$D_T(r) = \langle [T(\boldsymbol{x}) - T(\boldsymbol{x}+\boldsymbol{r})]^2 \rangle, \tag{2}$$

where $<\cdots>$ refers to an ensemble average.

$D_T(r)$ has a close relationship with C_T^2, which can be obtained as shown in Eq. (3):

$$D_T(r, h) = C_T^2(h) r^{2/3}, \; l_0 \ll r \ll L_0, \tag{3}$$

where h is the height of the sounding balloon, r is 1 m within the inertial subrange $l_0 < r < L_0$, l_0 is the inner scale, and L_0 is the outer scale.

With C_T^2, C_n^2 can be deduced from measured average $T\,(K)$ and $P\,(hPa)$ using the Gladstone formula [Eq. (4)] [21,22]:

$$C_n^2(h) = \left[79 \times 10^{-6} \frac{\mathrm{P}(h)}{T^2(h)}\right]^2 C_T^2(h). \tag{4}$$

3. METHODOLOGY

A. Models Derived from the Tatarskii Formula

Different models are utilized to estimate the C_n^2 profile, such as empirical and physically based parameterization approaches [23]. The simplest empirical methods using altitude as the only input parameter provide mean profiles of C_n^2, e.g., the CLEAR I model [24]. Considering the complexity of optical turbulence, it is obvious that only using altitude to quantify the turbulence strength is insufficient. In contrast, the parameterization methods derived from the Tatarskii equation contain more meteorological parameters, according to Eq. (5) [3,24]. Here, L_0, outer scale of turbulence (in m), is a crucial parameter, which is stated in Kolmogorov theory, M is the gradient of potential refractive index, and θ is the potential temperature. In this section, h is a.s.l. in all formulas:

$$C_n^2 = a L_0^{4/3} M^2, \tag{5}$$

$$M = \frac{\partial N}{\partial h} = -\frac{79 \times 10^{-6} P}{T^2} \frac{\partial \theta}{\partial h}, \tag{6}$$

$$\theta = T\left(\frac{1000}{P}\right)^{0.286}. \tag{7}$$

Some outer scale models, based on the Tatarskii formula, have been proposed to estimate C_n^2 profiles from different atmospheric parameters. A mean model developed by Colman and Vernin [25] treats the outer scale as a function of altitude between 2 and 17 km [Eq. (8), h in m]. Later, the expressions, for heights beyond 17 km and below 1 km, were supplemented by Beland and Brown [26] [Eq. (9), h in km] and Abahamid *et al.* [27] [Eq. (10), h in km], respectively. Hereafter, Eqs. (8)–(10) are referred to as the C-V model:

$$L_0(h) = \frac{4}{1 + \left(\frac{h-8500}{2500}\right)^2}, \; 2000 \text{ m} \le h \le 17000 \text{ m}, \tag{8}$$

$$L_0(h) = 0.307 - 0.0324(h-17) + 0.00167(h-17)^2 + 0.000476(h-17)^3, \; 17 \le h \le 30 \text{ km}, \tag{9}$$

$$L_0(h) = 3.21 h^{-0.11}, \quad 0 \le h \le 1 \text{ km}. \tag{10}$$

Another model was proposed by Dewan *et al.* [28] [Dewan model, Eq. (11)] by considering the vertical shear of the horizontal wind speed [S, Eq. (12)]. Two expressions for the troposphere and stratosphere are proposed. Trinquet *et al.* indicated the model needs to be used with a vertical resolution of 300 m, and S must not exceed 0.04 s^{-1} [29]:

$$L_0{}^{4/3}(h)=\begin{cases}0.1^{4/3}\times 10^{1.64+42\times S}, \text{ troposphere}\\ 0.1^{4/3}\times 10^{0.506+50\times S}, \text{ stratosphere}\end{cases}, \tag{11}$$

$$S=\left[\left(\frac{\partial u}{\partial h}\right)^2+\left(\frac{\partial v}{\partial h}\right)^2\right]^{1/2}. \tag{12}$$

Ruggiero and DeBenedictis [30] proposed the HMNSP99 model [HMN model, Eq. (13)], in which the outer scale is the function of S and temperature gradient ($\frac{dT}{dh}$) simultaneously. The authors believe that the model contained more atmospheric parameters and might be better in line with the nature of actual development of turbulence:

$$L_0{}^{4/3}(h)=\begin{cases}0.1^{4/3}\times 10^{0.362+16.728\times S-192.347\frac{dT}{dh}}, \text{ troposphere}\\ 0.1^{4/3}\times 10^{0.757+13.819\times S-57.784\frac{dT}{dh}}, \text{ stratosphere}\end{cases}. \tag{13}$$

B. Method of Statistical Analysis

To evaluate the performance and reliability of different models in reconstructing optical turbulence strength, two statistical operators are used, including the bias and root mean square error (RMSE) [31]:

$$\text{BIAS}=\sum_{i=1}^{N}\frac{(Y_i-X_i)}{N}, \tag{14}$$

$$\text{RMSE}=\sqrt{\sum_{\text{i}=1}^{N}\frac{(Y_{\text{i}}-X_i)^2}{N}}, \tag{15}$$

where X_i is the individual measured values of $\log(C_n^2)$, Y_{i} is the corresponding estimated values of $\log(C_n^2)$ by different models, and N is the number of samples for a couple (X_{i}, Y_i). Utilizing the bias and the RMSE, we retrieve the bias-corrected RMSE (σ):

$$\sigma=\sqrt{\sum_{i=1}^{N}\frac{\left[(X_i-Y_i)-(\overline{X_i-Y_i})\right]^2}{N}}$$

$$=\sqrt{\text{RMSE}^2-\text{BIAS}^2}. \tag{16}$$

Considering the actual value of C_n^2, basically in the range of $10^{-20}-10^{-13}m^{-2/3}$, using $\log(C_n^2)$ instead of C_n^2 makes it easier to calculate and visualize the statistical results, which makes the results more readable. This is just a substituted conversion to represent the error of C_n^2, so it is reliable and valid.

C. Integrated Astroclimatic Parameters

It is necessary to obtain r_0, ε, θ_0, and τ_0 to design and operate AO facilities. The visible ε is a crucial parameter that leads us to distinguish the most effective windows in the AO systems, which can be used to deduce r_0 [32]. Moreover, θ_0, which represents how much turbulence exists in the free atmosphere, especially for upper regions of the atmosphere, can be used to determine the ability to conduct applied optics experiments in a wide or narrow field [33,34]. In addition, the wind speed ($V(h)$) and C_n^2 profiles are used to calculate τ_0, which shows how fast the turbulence is [33]. All of the parameters are given as follows:

$$r_0=\left[0.423\left(\frac{2\pi}{\lambda}\right)^2\int_0^{\infty}C_n^2(h)\text{d}h\right]^{-3/5}, \tag{17}$$

$$\varepsilon_{\text{FWHM}}=0.98\frac{\lambda}{r_0}=5.25\lambda^{-1/5}\left(\int_0^{\infty}C_n^2(h)\text{d}h\right)^{3/5}, \tag{18}$$

$$\theta_0=0.057\lambda^{6/5}\left(\int_0^{\infty}h^{5/3}C_n^2(h)\text{d}h\right)^{-3/5}, \tag{19}$$

$$\tau_0=0.057\lambda^{6/5}\left(\int_0^{\infty}|V(h)|^{5/3}C_n^2(h)\text{d}h\right)^{-3/5}. \tag{20}$$

4. RESULTS

A. Comparison of the Considered Outer Scale Models for Individual Profiles

To better investigate the turbulence characteristics of Lhasa, three outer scale models are chosen here to estimate C_n^2 profiles, including Dewan, C-V, and HMN. The comparison of C_n^2 profiles between measurements and predictions using different models is depicted in Fig. 5. In order to ensure the comparability of data, the vertical C_n^2 profiles were resampled every 100 m using a moving average, in particular, the #6 balloon lost the data from the ground up to about 3 km a.g.l. For all models, the turbulence intensity near the ground is strong. The C-V model seems to predict unreasonable amplitudes of turbulence strength and inaccurate positions of turbulence layers. The Dewan model is more likely to overestimate the strength of

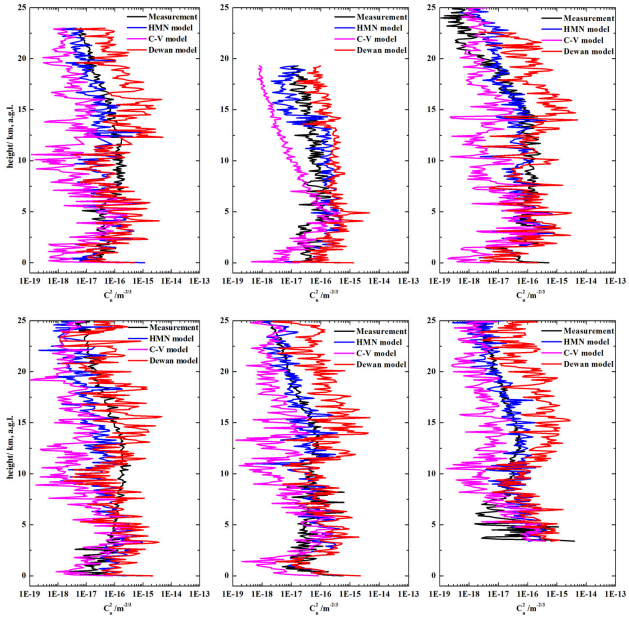

Fig. 5. Comparison of C_n^2 profiles between measurements by meteorological balloons and predictions by different outer scale models, including Dewan, C-V, and HMN, for six samples of individual balloons. On the y axis, the height a.g.l. is reported.

Table 2. Statistical Analysis of $\log(C_n^2)$ Calculated by HMN, Dewan, and C-V Models for Six Samples of Individual Meteorological Balloons

Balloon Number	Model	BIAS	RMSE	σ
1#	HMN	−0.23	0.65	0.61
	Dewan	0.41	0.89	0.79
	C-V	−0.97	1.24	0.78
2#	HMN	0.20	0.60	0.57
	Dewan	0.65	0.74	0.35
	C-V	−0.68	0.92	0.62
3#	HMN	0.04	0.64	0.64
	Dewan	0.69	1.21	0.99
	C-V	−0.65	1.15	0.95
4#	HMN	−0.37	0.78	0.69
	Dewan	0.24	0.85	0.81
	C-V	−0.95	1.24	0.79
5#	HMN	0.07	0.55	0.54
	Dewan	0.72	1.00	0.69
	C-V	−0.61	0.95	0.73
6#	HMN	0.16	0.61	0.59
	Dewan	0.88	1.10	0.67
	C-V	−0.53	0.88	0.70

turbulence at high altitudes. Overall, the estimated values of C_n^2 profiles using the HMN model are more consistent with the measured values than those of the Dewan and C-V models.

To quantify the above three outer scale performances, the statistical results for individual samples of $\log(C_n^2)$ between the measurements and model-based estimations are tabulated in Table 2. Among the three models, the HMN model has the lowest bias, RMSE, and σ for the #1, #3, #5, and #6 balloons, the lowest bias and RMSE, and second lowest σ for the #2 balloon as well as second lowest bias and the lowest RMSE and σ for the #4 balloon. In addition, the performance of Dewan and C-V models is difficult to distinguish. In conclusion, it is obvious that the HMN model shows more reliable C_n^2 profiles and better statistical results than those of the Dewan and C-V models.

B. Statistical New Model Performances

Previous studies have shown that optical turbulence is likely to be triggered by S and $\frac{dT}{dh}$ [30,35,36]. The results in Section 4.A further prove that the HMN model with the function of S and $\frac{dT}{dh}$ can better reveal the physical mechanism of optical turbulence. Therefore, using the meteorological balloons data at Lhasa, a new statistical outer scale model of Lhasa was derived from the HMN model. For comparison, another new statistical outer scale model was deduced from the Dewan model.

In detail, first, using the measurements obtained from balloons, the statistical average of vertical profiles of L_0, S, and $\frac{dT}{dh}$ are acquired with a vertical resolution of 100 m. Second, based on the HMN model, L_0, S, and $\frac{dT}{dh}$ are used to develop the new HMN model. At the same time, on the basis of the Dewan model, we use L_0 and S to deduce the new Dewan model. Finally, until the residual sum of squares between measured values and estimations are minimized, the two new outer models are obtained. In the following, we refer to the two models as the Lhasa HMN model [Eq. (21)] and the Lhasa Dewan model [Eq. (22)], respectively, where h is a.s.l. in m:

Table 3. Statistical Analysis of $\log(C_n^2)$ Calculated by Lhasa HMN and Lhasa Dewan Models for Six Samples of Individual Meteorological Balloons

Balloon Number	Model	BIAS	RMSE	σ
1#	Lhasa HMN	−0.28	0.60	0.53
	Lhasa Dewan	0	0.66	0.66
2#	Lhasa HMN	0.12	0.50	0.49
	Lhasa Dewan	0.27	0.47	0.38
3#	Lhasa HMN	−0.01	0.66	0.66
	Lhasa Dewan	0.11	0.77	0.77
4#	Lhasa HMN	−0.31	0.60	0.52
	Lhasa Dewan	−0.06	0.61	0.60
5#	Lhasa HMN	0.01	0.41	0.41
	Lhasa Dewan	0.28	0.62	0.56
6#	Lhasa HMN	0.11	0.53	0.52
	Lhasa Dewan	0.42	0.70	0.56

$$L_0{}^{4/3}(h) = \begin{cases} 0.1^{4/3} \times 10^{2.111-3.625\times S-68.031\frac{dT}{dh}}, \text{troposphere} \\ 0.1^{4/3} \times 10^{1.632+3.624\times S-43.093\frac{dT}{dh}}, \text{stratosphere} \end{cases}, \tag{21}$$

$$L_0{}^{4/3}(h) = \begin{cases} 0.1^{4/3} \times 10^{2.611-3.763\times S}, \text{troposphere} \\ 0.1^{4/3} \times 10^{1.596+2.885\times S}, \text{stratosphere} \end{cases}. \tag{22}$$

In this part, attention has been given to evaluate the performance of the newly proposed Lhasa HMN and Lhasa Dewan models. Table 3 presents the statistical results about the bias, RMSE, and σ of individual samples of $\log(C_n^2)$ between the estimations calculated by new models and the measurements. Among the two models, the Lhasa HMN model is accompanied with the lowest bias, RMSE, and σ for the #3, #5, and #6 balloons, the lowest RMSE and σ for the #1 and #4 balloons as well as the lowest bias for the #2 balloon. One can see that the Lhasa HMN model performs better than Lhasa Dewan model in reconstructing the optical turbulence intensity.

In addition, the overall statistics between the Lhasa HMN and Lhasa Dewan models derived from all six balloons are performed, as shown in Fig. 6, with the vertical profiles of the bias, the RMSE, and σ. In this section, N is the number of samples for a couple (X_i, Y_i) at each precise height. Because the #6 balloon lost data below 3 km a.g.l., we use $N = 5$ at each precise height below 3 km a.g.l. and $N = 6$ above 3 km a.g.l. In detail, the bias, RMSE, and σ are calculated based on the C_n^2 profiles with a vertical resolution of 100 m; then, a moving average over 1 km has been applied to the final profiles. Looking at Fig. 6, the absolute values of the bias of the Lhasa HMN model are lower than or equal to that of Lhasa Dewan model for most of time. Moreover, they are basically lower than 0.5 except for near the ground. The RMSE and σ of Lhasa HMN model are lower than that of Lhasa Dewan model for most of time as well as smaller than 0.8 and 0.7 all along the 25 km a.g.l., respectively.

In conclusion, in consideration of the individual and overall statistical analyses, the Lhasa HMN model with the function of $\frac{dT}{dh}$ and S is more reliable than the Lhasa Dewan model in reconstructing the strength of optical turbulence of Lhasa. To some extent, the new coefficients of the Lhasa HMN model represent the turbulence characteristics of the Lhasa outer scale model. In general, the difference between the HMN and Lhasa

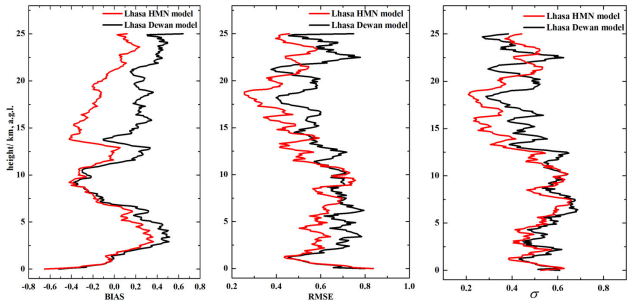

Fig. 6. Overall statistical analysis of $\log(C_n^2)$ profiles of six balloon samples. On the y axis, the height a.g.l. is reported.

Table 4. Comparison of Integrated Astroclimatic Parameters between the Radiosonde and Lhasa HMN Model[a]

Balloon	r_0 (cm)		$\varepsilon^{(\prime\prime)}$		$\theta^{(\prime\prime)}$		τ (ms)	
Number	Mea.	Mod.	Mea.	Mod.	Mea.	Mod.	Mea.	Mod.
1#	6.72	7.76	1.64	1.42	0.30	0.38	2.03	2.65
2#	8.18	5.65	1.34	1.95	0.42	0.31	2.92	2.06
3#	5.90	8.02	1.86	1.37	0.30	0.43	1.71	2.56
4#	5.57	7.82	1.97	1.41	0.25	0.41	1.20	2.11
5#	8.23	8.52	1.34	1.29	0.40	0.43	1.80	2.14
6#	8.12	9.23	1.35	1.19	0.46	0.44	2.89	2.46

[a]Mea. refers to measurement obtained from radiosonde; Mod. refers to estimation calculated from Lhasa HMN model, $\lambda = 0.55$ μm.

HMN models is mainly because the turbulence characteristics and turbulence profiles are different in different regions.

C. Comparison of Integrated Astroclimatic Parameters

In this section, we focus our attention to the ability of the Lhasa HMN model to rebuild r_0, ε, θ_0, and τ_0. The integrated astroclimatic parameters are obtained via C_n^2 values measured by balloons and estimated by the Lhasa HMN model. Because the #6 balloon lost some data near the ground, the corresponding integrated astroclimatic parameters are above 3 km a.g.l. The results are tabulated in Table 4. It is obvious that the Lhasa HMN model provides reasonable values, which are close to those measured by balloons. As we can see, the Lhasa HMN model is reliable in reconstructing integrated astroclimatic parameters.

5. CONCLUSIONS AND DISCUSSION

In this paper, the balloon-borne radiosondes are used to measure profiles of C_n^2 and atmospheric parameters such as T, P, RH, wind speed, and wind direction at Lhasa, south of the TP, for the first time. The comparison of turbulence strength between measurements obtained from balloons and predictions calculated by different outer scales including C-V, HMN, and Dewan models is conducted for six balloon samples at Lhasa. The statistical analysis result indicates that the HMN model has the best performance with the lowest bias, RMSE, and σ than the Dewan and C-V models.

Two new statistical outer-scale models, Lhasa HMN and Lhasa Dewan, are proposed using the balloon data of Lhasa. To evaluate the reliability of the two new models, statistical analysis for individual balloons of the C_n^2 profile between measurements and model-based estimations is carried out. It is apparent that the Lhasa HMN model presents the best level of performance with lower bias, RMSE, and σ than the Lhasa Dewan model. Meanwhile, to further verify the accuracy of the two models, we evaluate the overall statistics between Lhasa HMN and Lhasa Dewan models with six balloon samples. The absolute values of the Lhasa HMN model bias are basically lower than 0.5. Moreover, the RMSE and σ of the Lhasa HMN model are never greater than 0.8 and 0.7 all along the 25 km a.g.l., respectively, which are lower than those of the Lhasa Dewan model for most of the time. In general, the Lhasa HMN model is more reliable than the Lhasa Dewan model. This indicates that the Lhasa HMN model can better reflect the turbulence characteristics at Lhasa, which are closely related to local unique weather conditions. Furthermore, the Lhasa HMN model is applied to calculate integrated astroclimatic parameters, which provide reasonable values of r_0, ε, θ_0, and τ_0 as compared with the measurements obtained from balloon data.

The performance of the Lhasa HMN model is reliable and satisfactory in reconstructing strength of optical turbulence and integrated astroclimatic parameters at Lhasa. Considering the limited data, the Lhasa HMN model needs to be improved and perfected with more measurements. Therefore, further systematic investigations about turbulence characteristics at Lhasa are required. In general, it lays a foundation for the investigation of turbulence characteristics and astronomical site selection as well as provides support for the application of AO systems in the TP.

Funding. Strategic Priority Research Program of Chinese Academy of Sciences (XDA17010104); National Natural Science Foundation of China (91752103); Foundation of Key Laboratory of Science and Technology Innovation of Chinese Academy of Sciences (CXJJ-19S028).

Acknowledgment. The authors thank the Lhasa Meteorological Station for help in the field campaigns.

Disclosures. The authors declare no conflicts of interest.

REFERENCES

1. R. E. Good, R. R. Beland, E. A. Murphy, J. H. Brown, and E. M. Dewan, "Atmospheric models of optical turbulence," Proc. SPIE **928**, 165–186 (1988).
2. D. L. Hutt, "Modeling and measurement of atmospheric optical turbulence over land," Opt. Eng. **38**, 1288–1295 (1999).
3. V. I. Tatarskii, *Wave Propagation in a Turbulent Medium* (McGraw-Hill, 1961).
4. R. Stone, "World-class observatory rising on 'Roof of the World'," Science **337**, 1156–1157 (2012).
5. L. Y. Liu, Y. Q. Yao, J. Vernin, M. Chadid, Y. P. Wang, H. S. Wang, J. Yin, C. Giordano, and X. Qian, "Atmospheric turbulence measurements at Ali Observatory, Tibet," Proc. SPIE **8444**, 844464 (2012).
6. Y. Q. Yao, H. S. Wang, L. Y. Liu, Y. P. Wang, X. Qian, and J. Yin, "Site characterization studies in high plateau of Tibet," Proc. SPIE **8444**, 84441K (2012).

7. Y. Yao, Y. Zhou, L. Liu, H. Wang, J. Yin, X. You, and X. Fu, "Atmospheric monitoring strategy for the Ali site, Tibet," in *Journal of Physics: Conference Series* (IOP Publishing, 2015), p. 012038.
8. Q. Z. Ye, M. Su, H. Li, and X. M. Zhang, "Tibet's Ali: Asia's Atacama?" Mon. Not. R. Astron. Soc. **457**, L1–L4 (2015).
9. C. L. Kuo, "Assessments of Ali, Dome A, and Summit Camp for mm-wave observations using MERRA-2 reanalysis," Astrophys. J. **848**, 64 (2017).
10. X. Qian, Y. Q. Yao, H. S. Wang, Y. P. Wang, Z. Bai, and J. Yin, "The characteristics at the Ali Observatory based on radiosonde observations," Publ. Astron. Soc. Pac. **130**, 125002 (2018).
11. M. S. Li, Y. M. Ma, W. Q. Ma, Z. Y. Hu, H. Ishikawa, Z. B. Su, and F. L. Sun, "Analysis of turbulence characteristics over the northern Tibetan Plateau area," Adv. Atmos. Sci. **23**, 579–585 (2006).
12. C. H. Qing and Q. G. Rong, "Preliminary investigation on potential submillimeter astronomical sites in Ting-Ri, Tibet," Acta Astronom. Sin. **36**, 419–427 (1995).
13. L. G. Bian, X. D. Xu, L. H. Lu, Z. Q. Gao, M. Y. Zhou, and H. Z. Liu, "Analyses of turbulence parameters in the near-surface layer at Qamdo of the southeastern Tibetan Plateau," Adv. Atmos. Sci. **20**, 369–378 (2003).
14. Y. J. Zhang, P. X. Wang, W. G. F. Y. Q. Yao, L. R. Liu, and X. Qian, "Climate regionalization in China for astronomical observations," Scientia Sin.(G) **40**, 1302–1314 (2010).
15. Y. L. Huang, "Primary approach to the astronomical climate condition at Tibet Area," Publ. Yunnan Obs. **1**, 12–18 (1996).
16. S. G. Wang, S. Z. Lan, S. Y. Jiang, H. Q. Chen, G. R. Qi, Z. Y. Wang, Z. Li, and X. D. Liu, "Preliminary investigation on potential astronomical sites in Tibet," Publ. Shaanxi Astron. Obs. **12**, 1–17 (1989).
17. W. H. Shuai, *Research of Atmospheric Optical Turbulence Model* (National Astronomical Observatories, Chinese Academy of Sciences, 2012).
18. W. X. Qing, Q. G. Tian, P. Jiang, B. Chai, C. Qing, J. Cai, X. M. Jin, and H. Y. Zhou, "A new method of measuring optical turbulence of atmospheric surface layer at Antarctic Taishan Station with ultrasonic anemometer," Adv. Polar. Sci. **26**, 305–310 (2015).
19. C. Qing, X. Q. Wu, X. B. Li, W. Y. Zhu, C. H. Qiao, R. Z. Rao, and H. P. Mei, "Use of weather research and forecasting model outputs to obtain near-surface refractive index structure constant over the ocean," Opt. Express **24**, 13303–13315 (2016).
20. J. Cai, X. B. Li, G. W. Zhan, P. F. Wu, C. Y. Xu, C. Qing, and X. Q. Wu, "A new model for the profiles of optical turbulence outer scale and on the coast," Acta Phys. Sin. **67**, 014206 (2018).
21. V. I. Tatarskii, *The Effects of the Turbulent Atmosphere on Wave Propagation* (Israel Program for Scientific Translations, 1971).
22. R. S. Lawrence, G. R. Ochs, and S. F. Clifford, "Measurements of atmospheric turbulence relevant to optical propagation," J. Opt. Soc. Am. **60**, 826–830 (1970).
23. R. R. Beland, J. H. Brown, R. E. Good, and E. A. Murphy, "Optical turbulence characterization of AMOS, 1985," AFGL-TR-88-0153 (Air Force Geophysics Laboratory, 1988).
24. R. R. Beland, "Propagation through atmospheric optical turbulence," in *The Infrared and Electro-Optical Systems Handbook* (SPIE, 1993), Vol. **2**, pp. 157–232.
25. C. E. Coulman, J. Vernin, Y. Coqueugniot, and J. L. Caccia, "Outer scale of turbulence appropriate to modeling refractive-index structure profiles," Appl. Opt. **27**, 155–160 (1988).
26. R. R. Beland and J. H. Brown, "A deterministic temperature model for stratospheric optical turbulence," Phys. Scr. **37**, 419–426 (1988).
27. A. Abahamid, A. Jabiri, J. Vernin, Z. Benkhaldoun, M. Azouit, and A. Agabi, "Optical turbulence modeling in the boundary layer and free atmosphere using instrumented meteorological balloons," Astron. Astrophys. **416**, 1193–1200 (2004).
28. E. M. Dewan, "A model for C^2_n (optical turbulence) profiles using radiosonde data," PL-TR-93-2043 (Directorate of Geophysics, Air Force Materiel Command, 1993).
29. H. Trinquet and J. Vernin, "A model to forecast seeing and estimate profiles from meteorological data," Publ. Astron. Soc. Pac. **118**, 756–764 (2006).
30. F. H. Ruggiero and D. A. DeBenedictis, "Forecasting optical turbulence from mesoscale numerical weather prediction models," in *DoD High Performance Modernization Program Users Group Conference* (2002), p. 10–14.
31. E. Masciadri, F. Lascaux, and L. Fini, "MOSE: operational forecast of the optical turbulence and atmospheric parameters at European Southern Observatory ground-based sites–I. Overview and vertical stratification of atmospheric parameters at 0–20 km," Mon. Not. R. Astron. Soc. **436**, 1968–1985 (2013).
32. D. L. Fried, "Optical resolution through a randomly inhomogeneous medium for very long and very short exposures," J. Opt. Soc. Am. **56**, 1372–1379 (1966).
33. F. Roddier, J. M. Gilli, and G. Lund, "On the origin of speckle boiling and its effects in stellar speckle interferometry," J. Opt. **13**, 263–271 (1982).
34. D. L. Fried, "Anisoplanatism in adaptive optics," J. Opt. Soc. Am. **72**, 52–61 (1982).
35. F. H. Ruggiero, D. A. DeBenedictis, R. J. Lefevre, and S. A. Early, "Mesoscale modeling effects on optical turbulence parameterization performance," in *The 84th AMS Annual Meeting (Seattle, WA)* (2004).
36. X. Q. Wu, X. M. Qian, H. H. Huang, P. Wang, C. L. Cui, and C. Qing, "Measurements of seeing, isoplanatic angle, and coherence time by using balloon-borne microthermal probes at Gaomeigu," Acta Astronom. Sin. **55**, 144–153 (2014).